CORROSION SCIENCE AND TECHNOLOGY, Vol.31, No.3(2002), pp.247~253

Intergranular Corrosion of Separator in Molten Carbonate Fuel Cell in Cathode Gas Environments

Kyehyun Cho

School of Metallurgy and Materials, Yeungnam University
Kyungbuk, Korea 712-749

The corrosion of separator plate is one of the hot issues in molten carbonate fuel cell (MCFC) operation due to its aggressiveness and high temperature. To better understand the corrosion process in MCFC environment, electrochemical method as well as immersion test have been carried out. This paper describes the effect of the cell operation temperature (650℃) on the corrosion characteristics of the AISI-type 316L stainless steel in 62/38 Li/K eutectic melt in the cathode gas environment. After the solution treatment at 1,200℃ for 4 hours followed by the sensitization treatment at 650℃ for predetermined time, the corrosion behavior of the sensitized sample was analyzed by electrochemical method. AISI-type 316L stainless steel in MCFC environments with sensitization in cathode gas atmosphere demonstrates high rates of dissolution on the grain boundary due to weak passivity and active/passive transition in their polarization curve. The susceptibility to grain boundary attack is enhanced by increasing the sensitization time, however, the huge cavity formation due to higher dissolution along grain boundary occurs below deep bulk material in the vicinity of grain boundary. The X_{pass} values were lowered by increasing immersion time due to oxygen depletion inside cavity. Huge bulk metal attack in the vicinity of the grooves occurred can be understood in terms of the IR $>\triangle \phi^*$ criterions. The combination of Cr-depleted region due to sensitization and decreasing oxygen concentration from top to bottom of the oxide layer, could be explained as groove growth for sizable change of intergranular corrosion morphology.

Keywords : *MCFC, intergranular corrosion, IR, sensitization.*

1. Introduction

The molten carbonate fuel cell(MCFC) is going to commercializing stage for development. For this technology to be economically competitive in the market, studies have been focusing on long term durability of cell separator up to 40,000 hours. Among several lifetime limiting factors such as electrolyte loss, NiO dissolution and degradation of separator material, the problem of corrosion of separator seems to be the most crucial one in both technical and economical respects. Therefore, the understanding of the corrosion behavior of metals in MCFC environments is the key solution to solve a problem for engineering of MCFC stack. It is reported[1] that the separator in Li/K melts can perforate because of extensive localized corrosion allowing fuel and oxidant to react directly or increasing IR loss. In consequence, high cost material, for example austenitic stainless steel is required, which, to some extent, refrains MCFC from being commercialized.[2]

After a general discussion on corrosion of separator in MCFC operating condition by Donado et al.,[3] various research works with chromium,[4,5] nickel,[6] stainless steels,[7] nickel base alloys[8] and nickel-iron alloys[9] have been carried out either in MCFC gas atmosphere or in a carbonate melt to understand the corrosion process and to choose the right material for separators. The results of these studies[5,8,9] obtained by electrochemical measurements for the initial rate of corrosion as well as the beneficial effect of alloying element addition to the bulk metal on corrosion resistance of stainless steels and nickel base alloys. From the corrosion experiment with stainless steels in carbonate melt and anode gas environment, a dual-layered oxide structure comprising iron-lithium-oxide surface layer followed by an inner layer rich in Cr_2O_3, was observed.[7,10,11] Severe carburization of the alloy near the surface and sensitization of the bulk alloy were commonly observed, too. As Shores et al.[2] pointed out, however, the interpretation of these results must be very comprehensive because the real corrosion environment in MCFC operating condition is too complicated to be represented in a model experiment. Hence, a basic metallurgical aspect like sensitization effect should be taken into account to evaluate a separator material such as AISI-type 316L stainless steel.

Intergranular corrosion is caused by the result of sensitization, i.e., grain boundary precipitation of carbide when materials have a thermal cycle without providing sufficient time for chromium diffusion to fill the locally depleted region. The stainless steel can be suffering from inter-granular corrosion(IGC) due to sensitization in the range of 425 to 815°C. In this case, carbon and chromium in stainless steel diffuse to grain boundary to form Cr-rich $M_{23}C_6$ carbide leaving the Cr-depleted region nearby. This Cr-depleted region becomes more susceptible to corrosion than the rest of grain area. It was reported[12] that severe localized corrosion should occurs in the separator of MCFC.

At 650°C, usual MCFC operating temperature, separator made with austenitic stainless steel is readily sensitized to be attacked by IGC.[13,14] According to the sensitization diagram,[15] only 1 hour heating at 650°C could result in the sensitization of stainless steel of which carbon content is as low as 0.03%. Hence, AISI-type 316L stainless steel seems to be proper choice since its very low 'C' content is expected to make itself relatively free from sensitization. In aqueous media, AISI-type 316L stainless steel showed an excellent resistance against IGC.[16-18] However, IGC attack on AISI-type 316L stainless steel in MCFC operating condition have been reported.[11,19]

Therefore, this paper is intended to describe the effect of the sensitization and huge cavity dissolution on the corrosion characteristics of the AISI-type 316L stainless steel in 62/38 Li/K carbonate eutectic melt at 650°C. Electrochemical measurement by potentiodynamic method and morphological observation of samples immersed in carbonate melt are adopted as experimental methods.

2. Experimental

All samples with dimensions of 2cm × 2cm × 0.1cm, were washed in distilled water followed by ultrasonic degreasing in acetone. To obtain a mirror-like surface, they were polished with 240 grit sand paper and 0.05μm alumina powder. After vacuum sealing in quartz tubes, these samples went through the solution treatment at 1,200°C for 4 hours followed by cooling down to 650°C and aging for predetermined time periods(10, 100, 500 hours) for the sensitization treatment. Ice-water quenching process was adopted to avoid possible undesired change of the sample at the final stage of the heat treatment schedule.

The electrochemical tests were performed in a typical pot-cell system shown in Fig. 1 (a). The reference electrode and the counter electrode were made with a gold wire and a gold flag, respectively. A sensitized or non-sensitized sample was used as the working electrode, which was spot welded with gold wire. The reference gas was a mixture of 33% O_2 and 67% CO_2. And the atmosphere gas mixture was bubbled through an alumina tube in the carbonate melt. The composition of the cathode atmosphere gas mixture was the same as the reference gas mixture, and flow rate was 200cc/min. For anode gas atmosphere, 80/20 H_2 and CO_2 mixture was supplied at a flow rate of 200cc/min. Well dried 62/38(mole ratio) lithium and potassium carbonate mixture was put into a pure alumina crucible placed in an electric furnace. The electrochemical experiments were carried out when the temperature of the carbonate melt arrived at 650°C. The potentiodynamic method was applied at a scan rate of 0.1 mV/sec in the potential range from -1,400 mV to 400 mV. The measurements were recorded with an EG&G potentiostat/galvanostat Model 273A controlled by a computer running the M352 corrosion software.

The immersion tests were also carried out at the same pot-cell condition as shown in Fig. 1 (b). After the immersion tests, the samples were picked up from the carbonate melt and washed by an ultrasonic cleaner with distilled water. The corrosion behavior of AISI-type 316L stainless steel, common separator material in MCFC, was evaluated in this paper. Then surface morphology of each sample

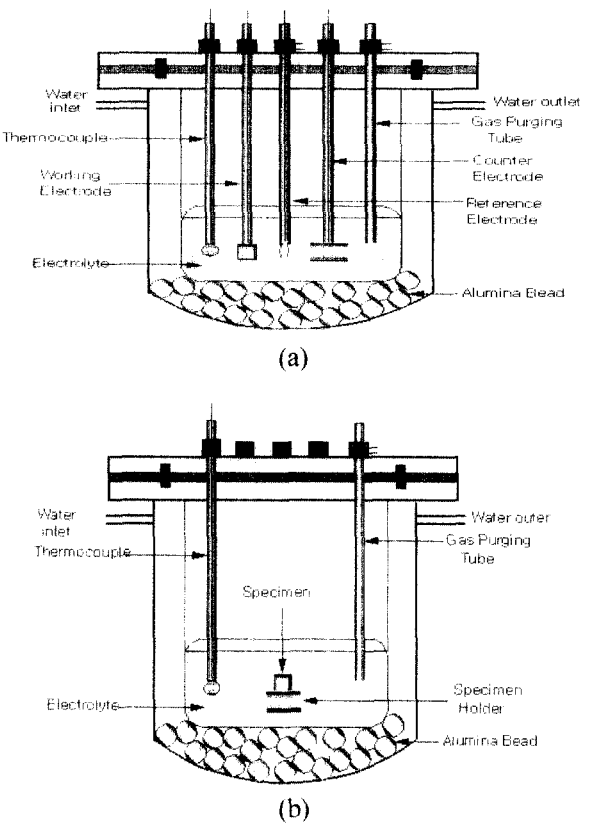

Fig. 1. Schematic diagram of pot-cell system. (a) electrochemical test and (b) immersion test.

was observed with optical microscope and SEM. In the vicinity of IGC due to sensitization, cross-section compositional analysis was accomplished by electron probe micro-analyzer (EPMA).

3. Results and Discussion

Fig. 2 shows polarization curves for samples from 0 hour sensitization treatment to 500 hours, obtained in cathode inlet gas atmosphere in a Li/K carbonate melt at 650℃. For 0 hour sensitization treatment, a polarization curve includes four typical regions: cathode, active, passive and transpassive regions, and its corrosion potential is about -1,020 mV. Around this corrosion potential, the measured potential-current density curves show relatively linear segments in both anodic and cathode direction, which are usually referred to as Tafel regions. At a potential of about -100 mV, so called the primary passivation potential, anodic peak current exists. Rapid corrosion rate takes place only when the actual electrode potential is more positive than the corrosion potential of the anodic reaction. Therefore, more positive the actual electrode potential becomes corrosion proceeds at a faster rate. However most transition metals have the passivity by forming protective oxide layer, which, in turn, produces passivation state even at more positive potentials than the corrosion potential. Above this potential, passivity begins, and the passive region appears over a wide range of potential where corrosion rate is usually very low. The transpassive region begins around 0 mV, where the current sharply increases. In contrast with the polarization behavior in the cathode gas atmosphere, corrosion potential in the anode gas atmosphere shifts to less noble direction by about 100 mV. A big difference between the two gas atmospheres is found in the passive region where the current measured in the cathode gas atmosphere shows much lower value.[12] The reason is because the stability of passive film strongly depends on oxygen concentration.

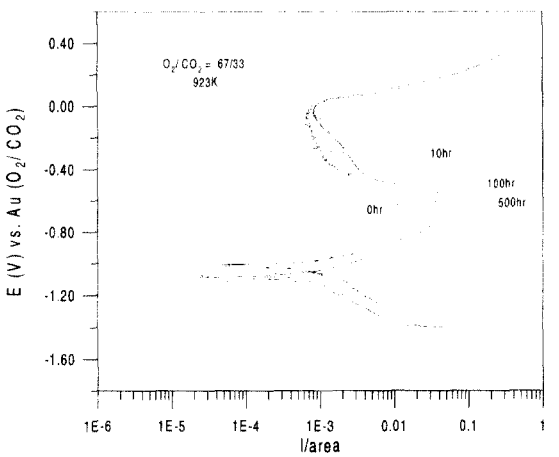

Fig. 2. Polarization curve of AISI-type 316L stainless steel in Li/K carbonate eutectic melt at 650℃ in cathode environments (scan rate = 0.1mV.sec)

In molten carbonate condition, predictable corrosion reactions can be represented for a metal M by the following equations;[3-6]

$$M \leftrightarrow M^{2+} + 2e^- \quad (1)$$

$$M + O^{2-} \leftrightarrow MO + 2e^- \quad (2)$$

$$M + 2OH^- \leftrightarrow MO + H_2O + 2e^- \quad (3)$$

$$M + CO_3^{2-} \leftrightarrow MO + CO_2 + 2e^- \quad (4)$$

Also, the electrochemical equilibrium of the cathode reaction for corrosion process can be expressed with the acid-base equilibrium of the Lux-Flood type reaction.[13,14] Therefore, the cathode reaction for corrosion process can be expressed as water reduction reaction or cathode reaction of carbonate ion as follow;

$$CO_3^{2-} \leftrightarrow CO_2 + O^{2-} \quad (5)$$

$$CO_3^{2-} + H_2O \leftrightarrow CO_2 + 2OH \quad (6)$$

From equation[5] and equation,[6] i.e., cathode reaction rate is very slow reaction compare to the anodic reaction and therefore the local equilibrium can be reached. So, it is reasonable that the corrosion rate of almost all metals decreases with decreasing CO_2 partial pressure. Based on the above equations, corrosion of stainless steel can proceed in two modes. First, a metal, M, can directly react with oxidizing ions in electrolyte as expressed in equations (2)-(4), producing an oxide layer. At a particular electrode potential, this oxide film begins to play a role of passive film. In such a case, the chromium oxide is known to be the most stable, protective oxide layer,[10-11] hence, the chromium content in a stainless steel is very important in determining the passivity in MCFC condition, too. Second, metal may directly dissolve out in the electrolyte by equation (1). This dissolution reaction may be accelerated when the electrode potential moves toward more positive direction. These corrosion reactions from equation (1) to equation (4) can be greatly affected by surroundings. For example, the composition of gas atmosphere is able to determine the corrosion phenomenon as a whole by controlling the stability of passive film and solubility of metal in a electrolyte. When dealing with corrosion problems of an MCFC under operation, this fact should be taken

Table 1. Summary of the electrochemical parameters by polarization curve

sensitization time(hr)	corrosion potential, V	corrosion rate	active peak current	comment
0	1.02	33mpy	23 mA/cm^2	
10	1.08	43mpy	31 mA/cm^2	
100	1.09	47mpy	85 mA/cm^2	
500	1.11	52mpy	120 mA/cm^2	

into consideration. Because the local environment of an MCFC cell frame varies from one location to another; e. g., wet seal area(anode, cathode), gas channel and current collector, etc., are exposed to different environments. In fact, the post analysis result, although not included in this paper, revealed a variety of corrosion in terms of type and severeness.[20]

Table 1 shows the effect of sensitization treatment time on polarization of AISI-type 316L stainless steel in cathode gas and in a carbonate melt. In spite of the fact that the sensitization effect is limited only in the vicinity of grain boundaries on the surface as shown in Fig. 3, the anodic peak current for without sensitization sample and 500 hours sensitization sample increases the current for 23 mA/cm^2 and 120 mA/cm^2, respectively. Also, passive current increases considerably over the entire passive range. For more detailed observation, these polarization curves are divided into three distinctive regions; equilibrium region, active region and passive region (polarization curves of Fig. 3 from 0 hour to 500 hours).

First of all, at the equilibrium region, the effect of sensitization treatment time on corrosion potential is remarkable. With increasing the degree of sensitization, the corrosion potential shifts to the less noble direction, namely, to more corrosion-susceptible state. This result is rather unexpected, considering the chromium depletion at grain boundaries due to sensitization and that chromium has more negative corrosion potential than nickel or iron. However, this result is in consistent with the previous result measured in an aqueous electrolyte by Ramamurthy et al..[21]

At the active region, the passive potential goes up slightly to anodic direction with the increase of the sensitization treatment time, and the peak corrosion current of the sensitized sample treated for 100 and 500 hours are higher by about 2.5 times than that of the non-sensitized sample. The similar result was observed by Osozawa et al.[22,23] in the aqueous electrolytes and it was concluded that the absence of passive film formation due to the depletion of chromium in the grain boundary areas was the reason for the higher peak current. Because the potential of the anode wet seal area of the MCFC imposed by its environmental usually belongs to this region, the corrosion resistance of this area will be significantly reduced by the sensitization which can not be avoided during an MCFC operation. When bare AISI-type 316L stainless steel was used, severe corrosion attack on anode wet seal area was observed, indeed.[24] Therefore, corrosion protection by a proper method such as aluminium coating on separator or adding inhibitor in electrolyte is indispensable.

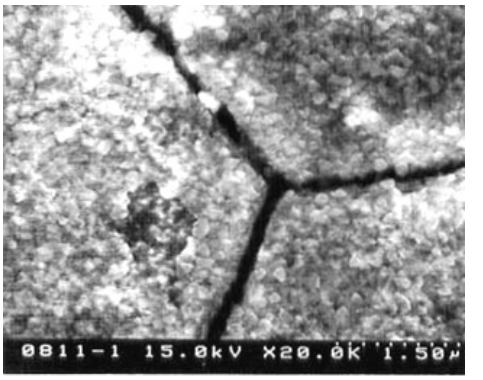

(a)

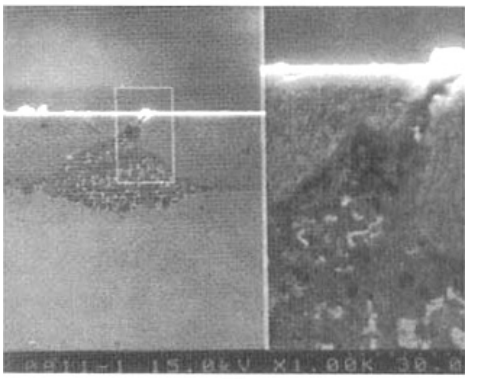

(b)

Fig. 3. SEM image of the surface. (a) and cross sectional SEM image and (b) of immersion tested sample for 200 hours.

At the passive region, by the same reason above, the corrosion current tends to increase with the increase of the sensitization treatment time. In a microscopic view, the passive state is a steady state between formation and dissolution of the passive oxide layer, so the increased corrosion current due to sensitization means that the stability of the passive film of the sensitized stainless steel is not as excellent as that of non-sensitized one. But the increment in corrosion current at the passive region which the environmental potential of cathode wet seal area belongs to, is not expected to cause such a serious corrosion problem as observed at the active region. According to the corrosion analysis after an MCFC operation, cathode

wet seal area made with bare AISI-type 316L stainless steel did not suffer extensively from corrosion attack but slightly from uniform corrosion.

Also, the effects of the sensitization treatment time on the corrosion rate and the corrosion potential are shown in Table 1. The corrosion rate in the equilibrium region was calculated by Tafel extrapolation method. With increasing sensitization treatment up to 100 hours, the calculated corrosion rate enhances very rapidly from 34 mpy to about 50 mpy, but stays at 50 mpy after that. This implies that the sensitization of AISI-type 316L stainless steel would be terminated in a short time. Very small amount of carbon content in this stainless steel could be one of the plausible reasons for the early termination of sensitization. Based on this observation, it can be concluded with caution that the direct effect of sensitization on corrosion, for example IGC, would not extend for a long time.

Fig. 3 (a) shows the SEM image of the surface of a non-sensitized sample after immersion test in a carbonate melt at 650°C for 200 hours. The regions in the vicinity of grain boundaries are severely attacked and dissolved out to produce deep grooves along grain boundaries which might be initiated due to chromium depletion by sensitization during the immersion period as explained previously. Some insights on the size as well as the morphology of grooves are likely to provide a clue for understanding the IGC observed in Fig. 3 (b) by SEM cross section micrograph. The very narrow groove of chromium carbide and Cr-free zone of 0.16㎛ wide strongly suggest that the chromium depletion region by chromium carbide formation is responsible for IGC. This result is remarkably comparable with others obtained in aqueous electrolytes system.[24] A recent study with a high resolution TEM has revealed the increase of chromium amount at grain boundaries due to chromium carbide precipitation leaving the Cr-depleted zone behind. Also, the kinetic model developed by Iyer et al.[25] and Bennett et al.[26,27] has predicted that the widths of Cr-depleted zone on each side of grain boundary and chromium carbide rich zone are 0.06㎛ and 0.04㎛, respectively, resulting in the total width of corrosion-susceptible area equal to 0.16㎛. This coincidence between the experimental and the calculated one is another evidence suggesting the role of Cr-depleted zone in IGC.

The X_{pass} change of corroded area of sample and its groove growth inside the cavity with increasing immersion time in a carbonate melt at 650°C are represented in Table 2. A schematic corrosion morphology as depicted in Fig. 4 (a) is one to one correspondence to SEM photographs in Fig. 3 (b), respectively.

The dissolution of the Cr-depleted areas near the grain boundaries but to dissolve the chromium carbide formed in the grain boundaries can be estimated the typical size of grain of the 316L stainless steel which is observed to be about 30㎛ for this experiments. The oxide layer of the sample immersed for 10 hours is relatively thin and

Table 2. Summary of the parameters for dissolution attack inside cavity with time

sensitization time(hr)	corrosion potential, V	corrosion rate	active peak current	comment
0	1.02	33mpy	23 mA/cm^2	
10	1.08	43mpy	31 mA/cm^2	
100	1.09	47mpy	85 mA/cm^2	
500	1.11	52mpy	120 mA/cm^2	

immersion time(hr)	X_{pass}	volume of cavity	comment
0	-	7.7 ㎛^{3}	Cr-depleted region
50	4.7 ㎛	256 ㎛^{3}	
100	3.1 ㎛	1125 ㎛^{3}	
200	2.5 ㎛	4170 ㎛^{3}	

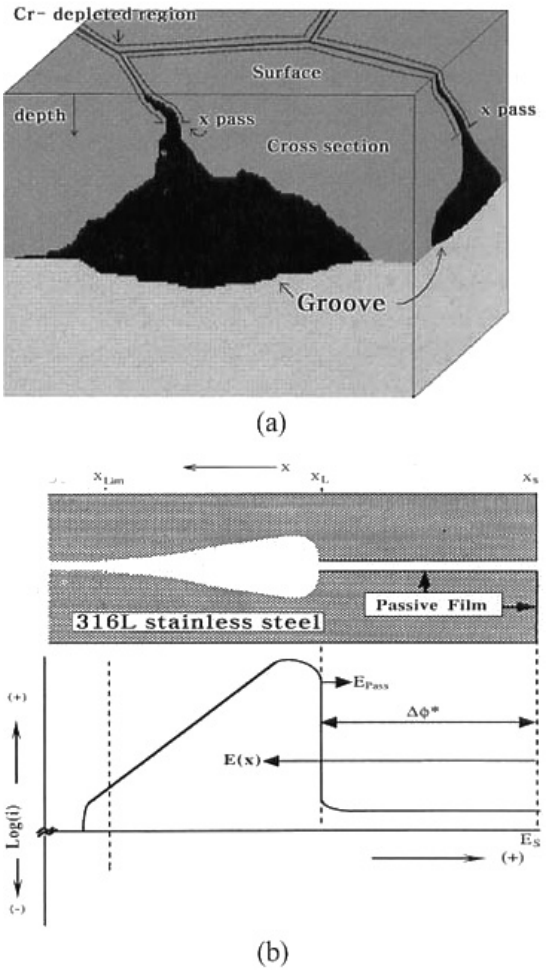

Fig. 4. A schematic drawing of corrosion attack on the cavity wall (a) and a schematic illustrations of the inter-granular attack and abnormal dissolution by IR induced inside cavity (b).

uniform with a thickness of 1.6㎛,[19] yet the groove between grains is not clearly visible. However, the thickness of oxide layer of the sample immersed for 50 hours reaches 5.3 ㎛ and the initiation of unexpected corrosion behavior at the interface between the oxide layer and the matrix can be observed as well. This interesting phenomenon of metal dissolution propagating from Cr-depleted grain boundary to the inside of oxide layer becomes distinct enough to cause the change in corrosion morphology, when immersion time elapses over 50 hours. The deeper from the surface, the groove width gets wider than that of expected value. In consequence, the initial groove shape turns into a cavity-like one after 100 hours in immersion. Fig. 3 (b) clearly shows that the interface, X_{pass} (corresponding to schematic drawings in Fig. 4 (a) which distinguishes the area under IGC attack from bulk metal dissolution exist and it moves upward to the surface with increasing the immersion time. The locations of X_{pass} at 50, 100 and 200 hours of immersion time are 4.7, 3.1 and 2.5㎛ below the surface, respectively. The large increase in the size of active peek with increasing sensitization time means that Xpass should decrease substantially with increasing sensitization time since the corresponding large increase in I and decrease in IR dominates over the constant in R in the IR $>\triangle \phi^*$ relations as shown in Fig. 4b. The higher dissolution cause a larger IR in the cavity thereby yielding the IR $> \triangle \phi^*$. In this case, IR $> \triangle \phi^*$ criterion represents that oxidant is depleted inside the cavity to cause metal dissolution whereas oxidant at the outer surface is plentiful in the passive state. After the potentiodynamic test, two samples, non-sensitized and 100 hours sensitized samples, were taken to examine their cross-sections by EPMA. The samples were well-developed oxide layers in the cross section micrographs indicating that very fast corrosions proceed. In this case the samples had been immersed in a carbonate melt with cathode gas atmosphere for only 5 hours. Obviously, the corrosion of the sensitized sample proceeds much faster than that of the non-sensitized one after potentiodynamic polarization test. These observations imply that the corrosion behavior of AISI-type 316L stainless steel in a carbonate melt can not be explained solely by the IGC mechanism but by the combination of the IGC and the classical localized corrosion, so-called crevice corrosion mechanism in an aqueous media,[30] in which the active/passive interface moves upward to the opening of cavity due to local environment changes as immersion time and the distance from the surface increases. In other words, the corrosion begins at the Cr-depleted area to produce grooves along the grain boundaries, but soon after bulk metal dissolution by the crevice corrosion mechanism takes over to create a large cavity in oxide layers. The exceptionally large bottom width and the volume of cavity after 200 hours in immersion which reaches up to 35㎛ and 4170㎛^{3}, respectively. The value was calculated on the assumption of cone shape for dissolved region, could be another evidence for this hypothetical combination of corrosion mechanism. The effect of oxidizing potential at the outer surface (E_{surf}) as shown in Fig. 4 (b) on the locations of passive and active metal dissolution (intergranular corrosion) inside the cavity is revealed in the cross section micrographs of the grooves. The oxidizing power is the amount of oxidant and/or its availability to the outer surface. If an oxidant had been used, the reduction rate could have been limiting. The role of oxidant discussed by Mcdonald et al.[28,29] who explain a decrease in the rate of crack propagation during stress corrosion by a decrease in availability of oxidant at the outer surface.

The reasons for the bulk metal dissolution are considered as follows: Relatively low oxygen concentration at the interface between the oxide layer and the matrix compared with that at the surface, is believed to play a responsible role in the bulk metal dissolution, just like its role in a typical crevice corrosion. Corrosion attack, even on a stainless steel, tends to proceed where oxygen activity or concentration is not high enough to make stable passive films. Furthermore, in this particular experiment, carbon dioxide concentration also contributes to determine the corrosion rate by controlling the basicity of a carbonate melt as well as participating in peroxide ion, O_2^{-2}, formation, as shown in equation.[5] It is well-known that the solubility of corrosion product strongly depends on the basicity of a carbonate melt and peroxide ion content directs the stability of a passive film.[31,32]

$$\frac{1}{2} O_2\,(gas) + CO_3^{2-} = O_2^{2-} + CO_2\,(dissolved) \qquad (7)$$

So far, observations and speculated reasons regarding corrosions on AISI-type 316L in a carbonate melt have been reported. But the details of corrosion mechanism associated with the bulk metal dissolution such as oxygen diffusion through grooves by IGC, peroxide ion concentration profile and etc., have yet to be investigated by the modelling work.

4. Conclusion

The intergranular corrosion of AISI-type 316L stainless steel in an MCFC environment has been investigated by polarization curve with different sensitization time and SEM micrographs on the sample surface and cross section micrographs after immersion in a Li/K carbonate melt.

1) AISI-type 316L stainless steel in MCFC environments with sensitization in cathode gas atmosphere demonstrates high rates of dissolution on the grain boundary due to weak passivity and active/passive transition in their polarization curve.

2) The susceptibility to grain boundary attack is enhanced by increasing the sensitization time, however, the cavity formation due to higher dissolution along grain boundary occurs below deep bulk material in the vicinity of grain boundary.

3) The X_{pass} values were lowered by increasing immersion time due to oxygen depletion inside cavity based on the cross section observation. The huge cavity formation after initial intergranular attack (grooves) is probably due to oxygen concentration profile as a result of mass transfer restriction through the grooves.

4) Huge bulk metal attack in the vicinity of the grooves occurred can be understood in terms of the IR $>\triangle\phi^*$ criterions. The active metal dissolution occurs since the oxidant is depleted inside cavity restricted by diffusion process whereas the oxidant is plentiful at the outer surface.

References

1. D. A. Shores and M. J. Pischke, *Proceedings of the Symposium in Molten Carbonate Fuel Cell Technology*, Edited by D. A. Shores and J. R. Selman, The Electrochemical Society, Pennington, NJ, p. 214 (1993).
2. K. Kinoshita, F. R. McLarnon, and E. J. Cairns, "Fuel Cells A Hand Book", Lawrence Berkeley Laboratory, CA, p. 64 (1988).
3. R. A. Donado, L. G. Marianowski, H. C. Maru, and J. R. Selman, *J. Electrochem. Soc.*, **131**. 2535 (1984).
4. H. S. Hsu and J. H. DeVan, *J. Electrochem. Soc.*, **133**, 2077 (1986).
5. J. P. T. Vossen, R. C. Makkus, and J. H. W. de Wit, *J. Electrochem. Soc.*, **143**, 66 (1996).
6. J. P. T. Vossen, L. Plomp, and J. H. W. de Wit, *J. Electrochem. Soc.*, **141**, 3040 (1994).
7. D. A. Shores and P. Singh, *Proceedings of the Symposium in Molten Carbonate Fuel Cell Technology*, Edited by J. R. Selman and T. D. Claar, The Electrochemical Society, Pennington, NJ, p. 271 (1984).
8. J. P. T. Vossen, L. Plomp, J. H. W. de Wit, and G. Rietveld, *J. Electrochem. Soc.*, 142, 3327 (1995).
9. J. P. T. Vossen, A. H. H. Janssen, and J. H. W. de Wit, *J. Electrochem. Soc.*, **143**, 58 (1996).
10. P. Singh and H. C. Maru, "*Stability of Iron and Nickel Base Alloys in Molten Carbonate Fuel Cell*". in Corrosion 85, NACE, Houston, Paper 344 (1985).
11. C. Y. Yuh, *Proceedings of the Symposium in Molten Carbonate Fuel Cell Technology*, Edited by D. A. Shores and J. R. Selman, The Electrochemical Society, Pennington, NJ, p. 368 (1993).
12. S. Hong, 'A Development of 2KW Molten Carbonate Fuel Cell Stack, KEPCO Report, 1995
13. D. A. Jones, "Principles and Prevention of Corrosion", 2nd ed., Prentice Hall, NJ, p. 292 (1996).
14. M. G. Fontana, "Corrosion Engineering", 3rd ed., McGraw-Hill, NY, p. 78 (1986).
15. R. M. Davison, T. DeBold, and M. J. Johnson, "Metals Handbook", Vol. 13, Corrosion, 9th ed., ASM, Metals Park, OH, p. 547 (1987).
16. R. Beneke and R. F. Sandenbergh, *Corrosion Science*, **29**, 543 (1989).
17. V. Ciahl, *Corrosion Science*, **20**, 737 (1984).
18. A. O. Majidi and M. A. Streicher, *Corrosion Science*, **24**, 393 (1984).
19. Yamamoto and S. Takahashi, *Proceedings of the Symposium in Molten Carbonate Fuel Cell Technology*, Edited by J. R. Selman and T. D. Claar, The Electrochemical Society, Pennington, NJ, p. 181 (1984).
20. "A Development of 2kW Molten Carbonate Fuel Cell Stack" Technical report, TR.93T-J03.97.01, Korea Electric Power Research Institute p.387 (1997).
21. S. Ramamurthy, A. Atrens, and I. O. Smith, Materials Science Forum, Vol. 44&45, Copyright Trans Tech Publications, Switzerland, p. 139 (1988).
22. K. Osozawa and H. J. Engell, *Corrosion Science*, **6**, 389, (1966).
23. K. Osozawa, K. Bohnenkamp, and H. J. Engell, *Corrosion Science*, **6**, 421 (1966).
24. R. G. Faulkner, *J. Material Science*, **16**, 373 (1981).
25. R. N. Iyer and H. W. Pickering, Environmental Degradation of Engineering Materials Conference, State College, PA (1987).
26. B. W. Bennett and Pickering, *Acta Metall.*, **36**, 539 (1988).
27. B. W. Bennett and Pickering, *Metallurgical Transactions A*, **18A**, 1117 (1987).
28. D. D. Macdonald, *Corrosion*, **48**, 194 (1992)
29. D. D. Macdonald, *Corrosion*, **52**, 768 (1996)
30. K. Cho, M. I. Abdulsalam, and H. W. Pickering, *J. Electrochem. Soc.*, **145**, 1862 (1998).
31. H. S. Hsu, J. H. DeVan, and M. Howell, *J. Electrochem. Soc.*, **134**, 2146 (1987).
32. H. S. Hsu and J. H. DeVan, *J. Electrochem. Soc.*, **134**, 3038 (1987).